UNIVERSITY OF CALIFORNIA SAN DIEGO

PTPRG Dimerization in Primary Dermal Fibroblasts

A thesis submitted in partial satisfaction of the requirements
for the degree Master of Science

in

Biology

by

Irene Vory Choi

Committee in charge:

Professor Nunzio Bottini, Chair
Professor Enfu Hui, Co-Chair
Professor Pradipta Ghosh
Professor Andres Leschziner

2022

The thesis of Irene Vory Choi is approved, and it is acceptable in quality and form for publication on microfilm and electronically.

University of California San Diego

2022

DEDICATION

In recognition of Dr. Nunzio Bottini for his enthusiasm and leadership in the development of science and training of scientists.

In recognition of Dr. Eugenio Santelli and Dr. Shen Yang for their wisdom, mentorship, and patience.

In recognition of Dr. William Kiosses who performed all microscopy image acquisition and whose help, instruction, and understanding has helped me gain a deeper appreciation for microscopy techniques.

In recognition of my parents for their constant love, understanding, and support – you have shaped me into the person I am today, and I am always grateful for you.

TABLE OF CONTENTS

LIST OF ABBREVIATIONS

AP FRET	Acceptor photobleaching Förster resonance energy transfer
D1	Domain 1
D2	Domain 2
ΔECD	Deletion of extracellular domain
FRET	Förster resonance energy transfer
mDF	Murine dermal fibroblast
pFRET	Parasamy Förster resonance energy transfer
pNPP	para-Nitrophenyl phosphate
PTPRG	Protein tyrosine phosphatase receptor type gamma
PTPRZ	Protein tyrosine phosphatase receptor type zeta
RPTP	Receptor protein tyrosine phosphatase
SE FRET	Sensitized emission Förster resonance energy transfer
TCPTP	T-cell protein tyrosine phosphatase
TGF-**β**1	Transforming growth factor - **β**1
WT	Wildtype

LIST OF FIGURES

ABSTRACT OF THE THESIS

PTPRG Dimerization in Primary Dermal Fibroblasts

by

Irene Vory Choi

Master of Science in Biology

University of California San Diego, 2022

Professor Nunzio Bottini, Chair
Professor Enfu Hui, Co-Chair

Fibrosis is a condition characterized by tissue overgrowth, hardening, and /or scarring. It is typically caused by excess deposition of extracellular matrix (ECM) components. Fibroblasts play an important role in the maintenance and reabsorption of the ECM, and thus can be critical mediators of the condition. Protein Tyrosine Phosphatase Receptor Type Gamma (PTPRG) is highly expressed in fibroblasts, and so we want to delve into how PTPRG activation and inactivation may play a role in the condition. The phosphatase activity of receptor-type protein tyrosine phosphatases (RPTPs) is widely thought to be regulated

through dimerization, however, the dimerization of PTPRG in fibroblast activity has not been seen in primary cells. Thus, we used FRET microscopy on a primary PTPRG knockout murine dermal fibroblast cell line (mDF) transfected with PTPRG mutant constructs to observe full-length protein dimerization in a cellular context. We also performed biochemical observations of protein activity through phosphatase activity experiments. We found that WT and several mutants of PTPRG dimerize in mDFs. A dimerization-inactivating mutant exhibits less dimerization in cells and in vitro.

INTRODUCTION

Fibrosis is a pathological feature seen in the end stages of most chronic inflammatory diseases; it is characterized by tissue hardening, overgrowth, and/or scarring which is typically caused by cells depositing excess extracellular matrix (ECM) components, such as collagen, fibronectin, and α-Smooth muscle actin (α-SMA) (Wynn, 2008). Fibroblasts in particular play a pivotal role in the maintenance and reabsorption of the ECM; in fibrosis, they can differentiate into myofibroblasts, which secrete ECM components and have migratory, contractile, and proliferative phenotypes which help generate the fibrotic phenotypes in tissue (Darby and Hewitson, 2007; Vallée and Lecarpentier, 2019). Because of this, fibroblasts are thought to be primarily responsible for fibrosis (Kendall and Feghali-Bostwick, 2014). Fibrosis can result from chronic inflammatory reactions induced by several conditions, including but not limited to autoimmune reactions, persistent infections, and tissue injury (Wynn, 2008). During these processes, many cytokines and growth factors may be secreted in a paracrine and/or autocrine manner. In particular, transforming growth factor-β1 (TGF-β1) experiences higher expression during fibrosis and has profibrotic effects on fibroblasts and fibroblast-type cells through canonical (ex. Smad2/3) and non-canonical (ex. MAPK, Rho-like GTPases) signaling pathways, making it a "master regulator" of fibrosis (Meng, 2016; Zhang, 2008). TGF-β1 plays a significant role in facilitating fibroblast differentiation into myofibroblasts (Vallée and Lecarpentier, 2019), which remain stably activated during fibrosis (Zehender et al., 2018). However, the molecular mechanisms of uncontrolled myofibroblast activation during pathogenic fibrotic responses are complex and require further investigation.

Several protein tyrosine kinases (PTKs) have been found to be promoters of profibrotic signaling and several PTK inhibitors are being investigated as potential anti-fibrotic agents in systemic sclerosis (Iwamoto, 2011); thus, this implies that protein tyrosine phosphatases (PTPs),

which counteract the activity of PTKs, may also play an important role in the progression or regression of fibrosis (Skhirtladze, 2008). Interestingly, Zehender et al. found that inhibition of Src homology 2 phosphatase (SHP2) actually inhibited TGFβ-induced fibroblast activation, and ameliorated dermal and pulmonary fibrosis. Similarly, previous work in the Bottini Lab discovered that Protein tyrosine phosphatase type IVA 1 (PTP4A1) promotes TGF-β1 signaling in fibroblasts as well as bleomycin-induced fibrosis in vivo; in the same study, it was observed that the mRNA of Protein Tyrosine Phosphatase Receptor Type Gamma (PTPRG) was highly expressed in dermal fibroblasts from 4 patients with diffuse cutaneous Systemic sclerosis (Sacchetti, 2017). Because of the acute role of fibroblasts in the development and pathogenesis of fibrosis, this spurred an interest in the potential role of PTPRG in fibrosis.

PTPRG is a classical transmembrane receptor-like tyrosine phosphatase (RPTP) that is composed of: an extracellular domain (ECD) with a carbonic-anhydrase-like (CAH) domain, fibronectin type III (FN III) domain and a spacer domain of unknown structure and function, a transmembrane region, and two intracellular domains (ICDs) known as domain 1 (D1) and domain 2 (D2), which is a common ICD structure found in RPTPs (Boni, 2021; Barr, 2009). PTPRG belongs to the R5 subgroup of RPTPs, along with PTPRZ (Alonso, 2004; Tonks, 2006). The phosphatase activity of PTPRG is in its ICD; D1 lies proximal to the membrane and performs the protein's catalytic phosphatase activity, whereas D2 is catalytically inactive and is thought to have regulatory and stability functions. The D1's catalytic activity relies on a common CX5R(S/T) motif that is found in many PTPs; the Cysteine residue in this sequence is found in the binding pocket in the center of D1 and can act as a nucleophile in catalysis (Tonks, 2006). RPTPs can regulate their phosphatase activity in D1 through intracellular dimerization that blocks the catalytic Cysteine. The ICD of Protein tyrosine receptor type alpha (PTPRA) has been

proposed to be organized in a symmetrical dimer with an "inhibitory helix-turn-helix wedge" motif that blocks the active site of the partner domain. PTPRG and PTPRZ, on the other hand, have been found in an alternate inhibitory homodimeric "head-to-toe" conformation (Tonks, 2006; Barr et al., 2009; Fujikawa et al., 2019) (Figure 1). In the case of dimeric PTPRG/Z, the catalytic Cysteine in D1 is blocked and thus provides an autoregulatory molecular basis for the inhibition of the phosphatase activity of the protein. Regarding the dimerization of PTPRG, Asp1305 and Asp1306 in the D2 domain were identified to provide important electrostatic interactions in the dimer interface; when both residues were mutated to lysine, the DDKK mutant was found to be monomeric in solution (Barr et al., 2009). The ECD of PTPRG could also play a role in regulating protein dimerization, as has been seen with PTPRZ (Fujikawa et al., 2019).

The dimerization of the ICD of PTPRG has been observed in-vitro through the resolution of its crystal structure (Barr et al., 2009). Still, it has not been observed with full-length protein in primary murine dermal fibroblasts using cellular biology approaches. In addition, the effects of dimerization on its activity have not been quantified.

Thus, the aim of our study was to witness PTPRG colocalization and dimerization using microscopy techniques and evaluate the effects of dimerization of PTPRG on its phosphatase activity. We used Förster Resonance Energy Transfer (FRET) microscopy between WT and mutant constructs of full-length PTPRG to study its dimerization habits, as well as to observe the localization of homodimeric PTPRG in the cell. FRET occurs when one excited fluorophore (donor) transfers energy to another fluorophore (acceptor) within 10 nm of it through long-range dipole-dipole coupling. The result is the fluorescence of the acceptor fluorophore. Positive FRET signal suggests an association, or in this case dimerization, between the proteins the donor and acceptor fluorophores are attached to. FRET microscopy can ultimately be used to visualize

the localization of dimers in the cell, and with additional analysis quantify FRET signaling for comparison between different samples (Shrestha et al., 2015). The mutants included in FRET microscopy experiments were: DDKK, a dimerization-inactivating mutant previously explained, ΔECD: a mutant with a deletion of the extracellular domain, and CS: a mutant that alters the catalytic Cysteine in D1, deactivating the phosphatase activity of the protein (Barr et al., 2009; Tonks, 2006). FRET image acquisition was performed by Dr. William B. Kiosses at The La Jolla Institute of Immunology. He is an expert in FRET-based microscopy and has optimized the technique to study protein-protein interaction and dimerization (Tzima et al., 2002; Tzima et al., 2005; DelPozo et al., 2002; Sendo and Kiosses et al., submitted for publication 2022).

In order to confirm the effect of the DDKK mutation on ICD dimerization and the potential subsequent increase in enzymatic activity, we performed phosphatase activity assays with purified D1D2 WT and DDKK protein using pNPP as a substrate. The data from these experiments suggested that the D1D2 WT protein was dimerizing at a greater rate than the D1D2 DDKK protein. To further clarify if the DDKK mutation was indeed affecting the dimerization of the intracellular domain of the protein, a co-immunoprecipitation (co-IP) was performed with purified proteins.

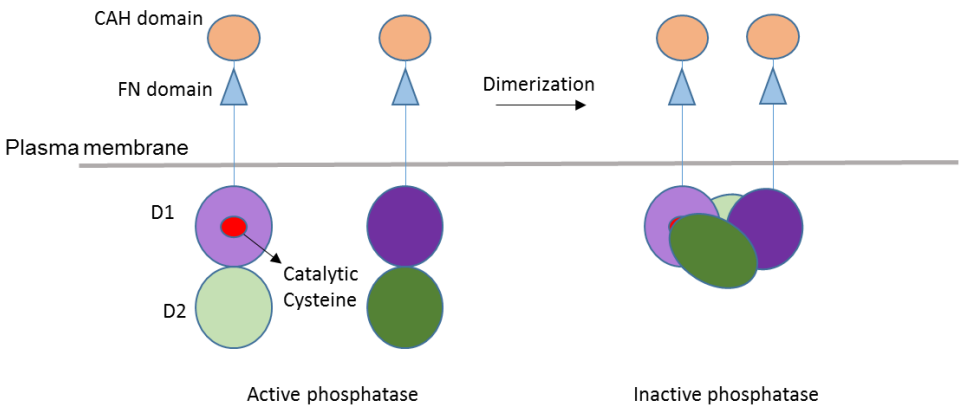

Figure 1: A scheme of PTPRG's proposed "head-to-toe" dimeric conformation.

MATERIALS & METHODS

Antibodies

Primary:

Mouse anti-FLAG antibody (F3165) - Sigma Aldrich

Rabbit anti-HA antibody (C29F4) - Cell Signaling Technology

Rabbit anti-FLAG antibody (D6W5B) - Cell Signaling Technology

Secondary:

Goat anti-mouse IgG Alexa Fluor 568 conjugate antibody (A11004) - Invitrogen

Direct Conjugates:

Mouse anti-HA Alexa Fluor 488 conjugate antibody (2350S) - Cell Signaling Technology

AF647 Phalloidin (A22287) - Invitrogen

Mouse Primary Dermal Fibroblast Isolation

Skin biopsies were obtained from PTPRG KO mice, washed twice with 70% ethanol, and transferred to tubes with Dulbecco's minimal essential medium (DMEM) (Corning), antibiotics (Penicillin/Streptomycin - Corning), and anti-mycotic (Gentamicin - Gibco). Skin biopsies were washed with DPBS (Fisher), then transferred into 6-well plates (Corning). A digestive enzyme mix of 0.2% Collagenase (Sigma Aldrich) and 2.4 units/mL Dispase (Roche) in previously described DMEM media was added to the skin punches before scissors and a scalpel blade were used to physically mince the skin to fine pieces. Additional enzyme digest mix was added to the well, and the mixture was allowed to digest for 2-3 hours at 37°C in a sterile cell culture

incubator. The plate was shaken approximately every 30 minutes. After digestion was complete, contents were washed with full primary mDF media (DMEM, 10% fetal bovine serum (FBS) (Atlanta Biologicals), 1% L-Glutamine - Gibco, 1% Penicillin-Streptomycin, and 0.1% Gentamicin), centrifuged then resuspended again in fresh primary mDF media before being plated in a 6-well plate. The cells were allowed to grow for 2 days before the media was changed.

Cell Culture and Transfection

Cells were grown in DMEM supplemented with 10% FBS, 2mM L-glutamine, 100 I.U. penicillin and 100ug/mL streptomycin, and 50ug/mL Gentamicin. Cells were kept at 37°C at 5% CO_2 in a sterile incubator. Transfections were performed using FuGENE HD reagent once the monolayer reached 80-90% confluency. Transfection media was DMEM with no additional additives. For microscopy experiments, the media was replaced with mDF growth media 12 hours post-transfection.

Confocal FRET Imaging

Ptprg KO primary mDFs were directly plated onto coverslips and allowed to grow to 90% confluence in 24-well plates. Cells were then transfected as described above. 48 hours after transfection, cells were fixed with 4% paraformaldehyde for 20min, permeabilized with 0.2% Triton X-100 and 1% BSA, blocked with normal goat serum (Life Technology), then stained with primary, secondary, and direct-conjugate antibodies. The slides were mounted onto slides with molecular probe gold reagent (Life Technology). The images were acquired and the technique was tested by our collaborator Dr. William B. Kiosses at the La Jolla Institute for Immunology (Tzima et al., 2002; Tzima et al., 2005; DelPozo et al., 2002; Sendo and Kiosses et

al., submitted for publication 2022). Using a Zeiss laser scanning confocal microscope 880 with a 63x (1.46 NA) and a 63x (1.4 NA) objective using the 32-channel GaAsP-PMT area detector, sensitized emission confocal FRET (SEcFRET) and spectral-based acceptor photobleaching (AP FRET) were used to capture images. The donor channel (488 excitation, 508-535 emission) and acceptor channel (568 excitation, 588-624 emission) were captured sequentially. A dynamic intensity range (0-4096) was determined using a population of WT cells that expressed moderate to the brightest signal of HA and FLAG-tagged PTPRG and was kept the same for all following image acquisition. The system settings were also defined and set based on the same WT controls: 1% laser power for the acceptor, 2% for both FRET channel and donor channels, and 800 for digital gain in donor, acceptor, and raw FRET image acquisition. Donor-alone, acceptor-alone, and donor-acceptor samples were taken for every experiment for later background fluorescence subtraction and spectral bleed-through correction factors in raw, uncorrected FRET samples in ImageJ. An automated, scripted SEcFRET method that had been developed earlier for widefield and confocal platforms was used (Hodgson et al, 2010, Kraynov et al., 2000, Chamberlain et al., 2000, Del Pozo et al., 2002; Tzima et al., 2002). Additionally, % FRET efficiency was calculated using Amassi Periasamy's method of precision FRET (pFRET) that was developed and scripted at UVA (Elangovan et al., 2003; Periasamy et al., 2008; Sun et al., 2013; Chen et al, 2007). For AP FRET, donor and acceptor fluorescence were tracked for 6 unbleached scans to establish stable fluorescence at each selected ROI, then monitored over a time regimen of 30 cycles (about 300s) after acceptor bleaching. FRET efficiency was then calculated by measuring the difference between quenched donor signal in the presence of the acceptor, and the de-quenched donor signal once the acceptor had been bleached (Chen et al., 2007, Bastiaens & Jovin, 1996; Wouters et al., 1998; Day et al., 2001; Zal et al., 2004). In this method calculation, each cell served as its

own control. The photobleaching module was used in the Zen Black software, and the following ROIs were selected: whole cell, two regions of cellular interest defined by the presence of actin fibers or lamellipodial edge (one region to photobleach, the other to serve as an unbleached control), and an area devoid of cells to act as the background control. The software tracks mean changes in fluorescence intensity within ROIs, which is then used to calculate the % FRET efficiency.

Cloning, Mutagenesis, Protein Expression and Purification

Codon-optimized ORF encoded the D1D2 fragment of mouse PTPRG (residues 824-1445), was subcloned into NcoI/XhoI sites of pET28a (Novagen) and expressed in *Escherichia coli* BL21 (DE3) as a C-terminal 6-Histidine fusion. N-terminal Flag or HA-tagged clones and other mutant clones were amplified from mouse full-length cDNA then cloned into the NcoI/XhoI site of pET28a. Bacterial cultures were grown at 37°C then induced with isopropyl 1-thio- ß-d-galactopyranoside at room temperature for more than 12 hours. The soluble fraction was recovered from the cell extract via centrifugation, and D1D2 PTPRG was purified via Ni-NTA affinity chromatography (Qiagen) followed by anion exchange on a HiTrap Q HP chromatography column (Cytiva). WT, CS, and ΔECD eukaryotic plasmids encoding full-length (or truncated for ΔECD) mouse PTPRG with an HA epitope tag at the C-terminus in pCDNA3.1(+) at restriction sites NheI/EcoRV were ordered from Mutagenex. Other mutant constructs were obtained by standard site-directed mutagenesis techniques, and mutations were confirmed by DNA sequencing. The primers used for mutagenesis were synthesized by Integrated DNA Technologies.

Phosphatase Activity Assays

For assays with pNPP as the substrate, protein was diluted to 20nM or 2uM in buffer 1xMM (50mM Tris pH7.3, 1mM dTT, 0.01% Triton X-100) and various concentrations (5mM, 2.5mM, 1.25mM, 0.5mM, 0.25mM, 0.125mM, 0.05mM, 0mM) of pNPP (Thermo Scientific) also diluted in buffer 1xMM. 25uL of protein solution and 25uL of pNPP solution were mixed in a 96-well solid flat clear-bottom polystyrene microplate (Corning) every 5 minutes over 35 minutes for assays performed with 20nM of protein solution, and every 10 seconds over 1 minute for assays performed with 2uM of protein solution. The reaction was terminated by adding 100uL of 1M NaOH. pNP formation was monitored by fluorescence measurement at a wavelengths of 405 nm on a Tecan Infinite M1000 plate reader. The initial reaction rates were fitted to a Michaelis-Menten equation on GraphPad Prism 8.

In Vitro Co-Immunoprecipitation

N-terminal FLAG or HA-tagged PTPRG D1D2 WT ($PTPRG^{WT}$) or DDKK ($PTPRG^{DDKK}$) plasmid and protein were obtained using the methods described in the section above called "Cloning, Mutagenesis, Protein Expression and Purification**."** The buffer used for rocking and washing was: 0.05% NP-40, 50mM Tris pH 7.5, 150mM NaCl, 0.1mM PMSF, 10mM EDTA pH 8.0, and 1 protease inhibitor pellet (Thermo Scientific). FLAG-tagged $PTPRG^{wt}$ (FLAG-$PTPRG^{WT}$) was rocked with anti-FLAG magnetic beads (Sigma) in buffer, washed, and then had either HA-tagged $PTPRG^{WT}$ or $PTPRG^{DDKK}$ (HA-$PTPRG^{WT}$ or HA-$PTPRG^{DDKK}$, respectively) protein added before the protein-bead solution was rocked and washed again. The co-immunoprecipitated proteins were eluted from the beads using sample buffer with SDS and b-mercaptoethanol and subjected to western blotting.

Western Blot

Samples were run at 120 mA for 1.5 hours through 4-20% Tris-Glycine mini protein gels (Novex), then transferred to nitrocellulose membrane at 40 V at 60°C for 1.5 hours. Primary antibodies were diluted 1:1000 in 5% milk, and the secondary antibody was diluted 1:5000 in 5% milk.

Statistical Analysis and Software

The Zen Black software was used to separate confocal multi-images into individual images for additional processing and data analysis. On ImageJ, a pFRET plug-in from the Periasamy group at UVA (Periasamy et al., 2008) was used for pFRET analysis. The SEcFRET macro was developed by Dr. William Kiosses and others at the La Jolla Institute of Immunology and Scripps Research Institute. The two-tailed Mann-Whitney test was used for statistical analysis in Graphpad Prism 8 after the data was gathered and analyzed (referred to as "post-hoc" in subsequent figure captions).

RESULTS

WT and catalytically inactive CS mutant PTPRG dimerizes and localizes along actin fibers in primary mDFs while the DDKK dimer-inactive and ECD KO mutant do not

FRET based microscopy, which is an ideal technique for studying intracellular molecular interactions with nanometer spatial resolution, was performed in order to visualize WT and mutant full-length protein localization and dimerization in primary cells. Understanding this could provide a greater understanding of how mutations affect PTPRG dimerization, and how the phosphatase activity and structural features of PTPRG might affect the fibroblast phenotype. PTPRG KO mDFs were transfected with both C-terminal FLAG and HA-tagged versions of WT and mutant PTPRG constructs. Cells were fixed, permeabilized, and stained with antibodies (donor, HA - AF488 and acceptor, FLAG - AF568) 48 hours after transfection. Cells for FRET studies were selected among ones exhibiting relatively equal levels of FLAG and HA expression based on the intensity of emissions of the respective fluorophores. FRET occurs when donor and acceptor fluorophores are within 10nm of each other (Shrestha et al., 2015). All images of cells had characteristic phenotypes of a spreading or migrating cell, focusing on leading edge lamellipodia, polarized stress fibers, and focal adhesions that were parallel to the leading lamellipodium. Lamellipodial edges are sites of actin polymerization below the leading plasma membranes of cells and are thought to play an important role in cell locomotion (Sixt, 2012). Fibroblast movement is especially important in fibrosis around a wound, in which stimulation by cytokines, growth hormones, etc. enhances cellular differentiation and migration toward the wound. In turn, the migrating cells remodel the ECM in the ways typically seen in fibrosis (Vallée and Lecarpentier, 2019). Three FRET image acquisition methodologies — SEcFRET,

pFRET, and AP spectral FRET — were performed in order to confirm PTPRG dimerization events between the different mutants.

Figure 2 shows the PTPRG-HA (green) and PTPRG-FLAG (red) signals individually, as well as merged (yellow), in order to visualize similar localization patterns of the two constructs for WT and mutant proteins. Once similar localization of the constructs was confirmed, SE confocal FRET analysis was performed to produce an image displaying FRET signaling patterns. The processed SEcFRET images are displayed as 8-bit and pseudo-colored to represent the regions of lower (dark blue) and higher (cyan/green) FRET signal. The areas of high FRET signal were localized around actin fibers as seen in the merged SEcFRET/phalloidin images for WT and CS mutant, while the SEcFRET images for the DDKK and ΔECD mutants showed more diffuse FRET signaling, which pointed toward decreased PTPRG dimerization on the actin fibers (Figure 2). Additionally, the DDKK and ΔECD mutants exhibited slightly weaker actin fiber formation than the other PTPRG constructs, as seen by a lack of strongly defined lines running through their phalloidin images.

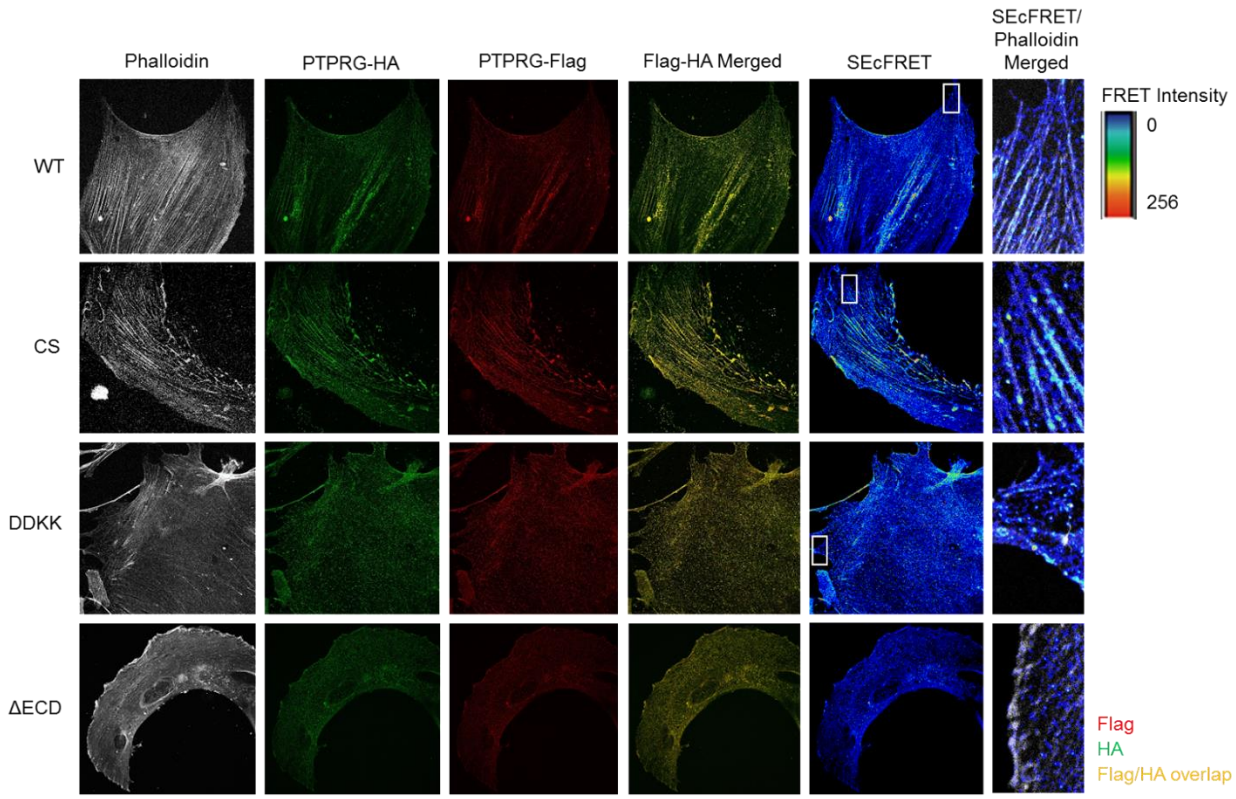

Figure 2: Full-length WT and CS mutant exhibit increased SEcFRET signal on actin fibers while ΔECD **and DDKK mutant exhibit diffuse SEcFRET signal.** Primary mDFs from PTPRG KO mice were transfected with FLAG and HA-tagged PTPRG WT or mutant constructs. Samples were imaged for FLAG (red), HA (green), phalloidin (white), and Hoechst (not shown). HA and FLAG signals were merged to show protein localization, indicated by yellow signal. Corrected SEcFRET images are presented with a heat map displaying the 0-256 dynamic range. Regions of interest are identified in SEcFRET with white boxes and zoomed-in to display a merged image of SEcFRET and phalloidin stain. Images are representative of two experiments (WT) or one experiment (CS, DDKK, and ΔECD) with n = 27-30 for each experiment.

pFRET analysis was used to calculate % FRET efficiency for each WT or mutant sample (Chen et al., 2007; Periasamy et al., 2008; Sun et al., 2013). pFRET analysis, though not typically used for FRET image generation, still showed similar FRET patterns for the WT, CS, DDKK and ΔECD mutants in regards to showing stronger dimerization patterns following actin fibers (WT and CS) or being more diffuse (DDKK and ΔECD) (Figure 3A). This verified that the two different analysis methods were tracing similar patterns between the different mutants. In addition, WT PTPRG exhibited greater % FRET efficiency compared to the DDKK mutant (Figure 3B). Meanwhile, the ΔECD mutant showed no significant difference in % FRET efficiency compared to WT PTPRG, while the CS mutant showed slightly decreased % FRET efficiency.

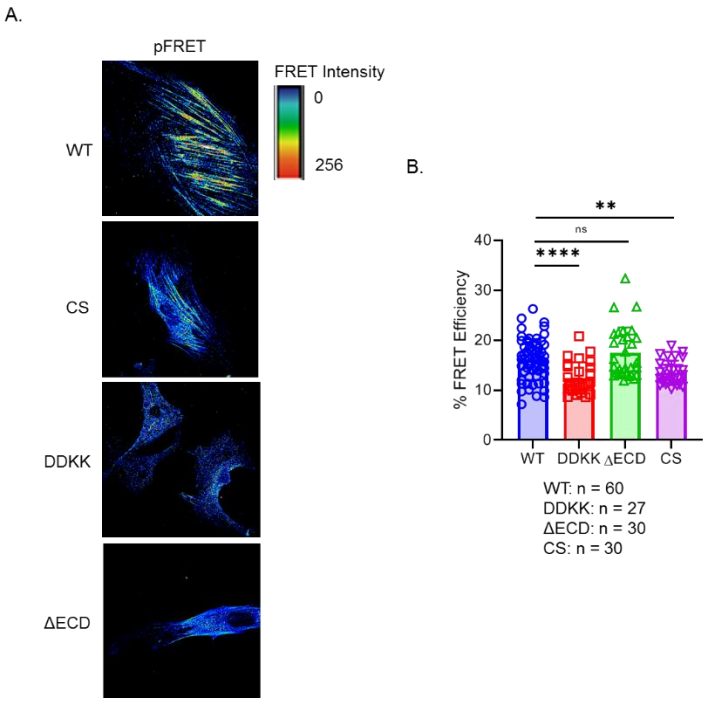

Figure 3: pFRET analysis shows full-length WT and ΔECD mutants exhibit similar % FRET efficiency while CS and DDKK mutant exhibit decreased efficiency. Primary mDFs from PTPRG KO mice were transfected with FLAG and HA-tagged PTPRG WT or mutant constructs. Samples were imaged for FLAG (red), HA (green), phalloidin (white), and Hoechst (not shown). FRET signal was collected at 568nm after excitation at 488nm. (A) pFRET analysis methodology was used to generate FRET images, along with a heat map displaying the 0-256 dynamic range (B) Data were analyzed to obtain % FRET efficiency using pFRET methodology. Figures are representative of two experiments (WT) or one experiment (CS, DDKK, and ΔECD) with n = 27-30 for each experiment. The Kruskal-Wallis test was used for statistical analysis along with the two-tailed Mann-Whitney post-hoc test (**** = $p < 0.0001$, ** = $p < 0.005$).

In AP FRET, regions of interest (ROI) of the cell were selected as described previously. AP FRET was performed by measuring the difference between the quenched donor signal when the acceptor was present, and the de-quenched donor signal once the acceptor was photobleached (Zal, 2004). Two ROIs were selected with one being bleached and the other as an unbleached control, as well as an area devoid of cells to act as a background control.

Mean changes in the donor fluorescence intensity were used to calculate % FRET efficiency. This was performed on the same sample of cells prepared for the previous FRET experiments. Figure 4A shows a sample of the donor (PTPRG-HA) and acceptor (PTPRG-Flag) fluorescence before and after the acceptor is photobleached, as well as a similar sample of a specified actin fiber ROI. Figure 4B shows that in the whole bleached ROI, WT, CS, and ΔECD PTPRG exhibited greater % FRET efficiency than the DDKK mutant, though there was no significant difference between WT/ΔECD or WT/CS.

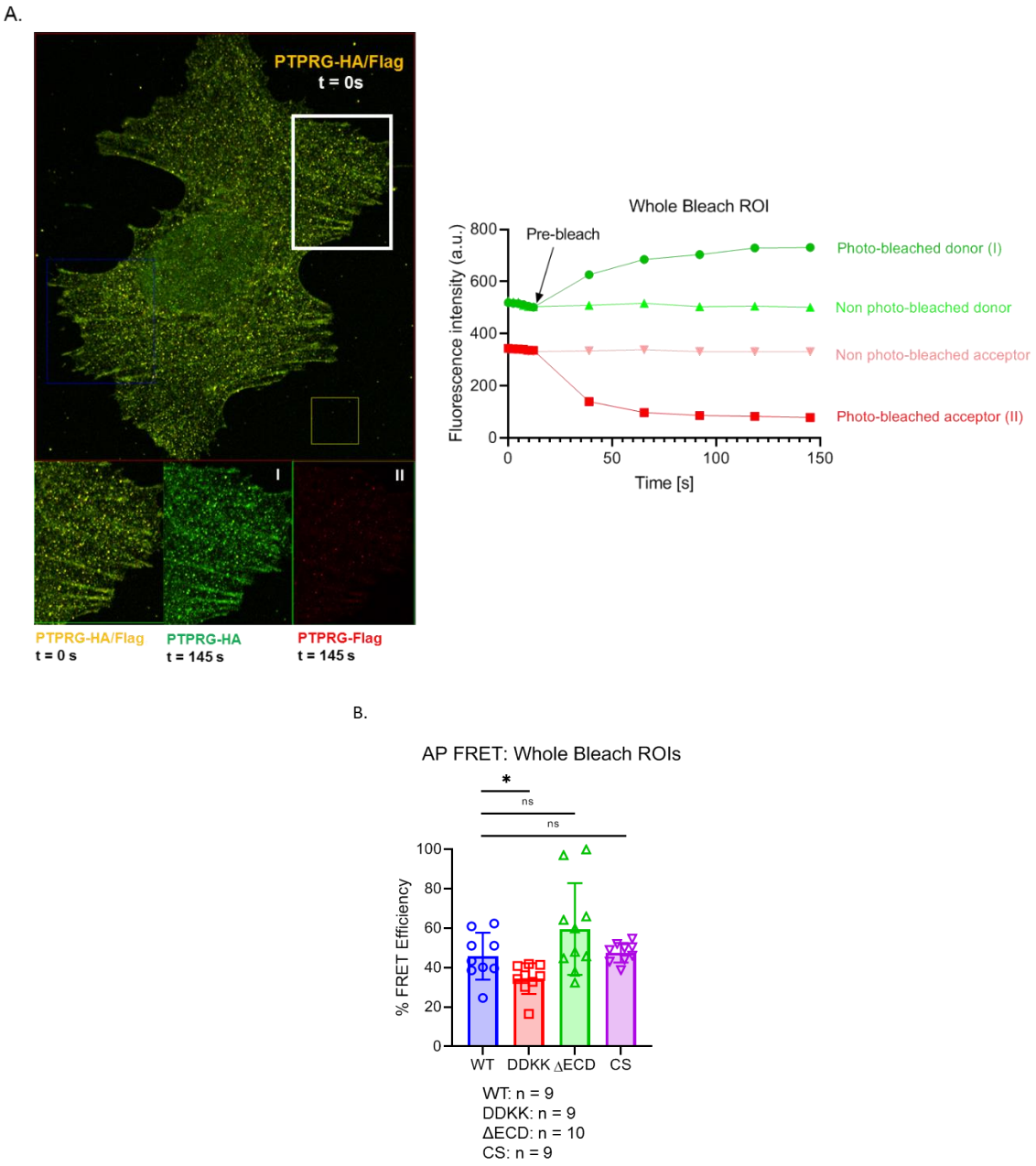

Figure 4: AP FRET analysis shows full-length PTPRG exhibits similar (WT, ΔECD, CS) or decreased (DDKK) % FRET efficiency in whole photobleached regions. (A) A region of the cell was imaged at t = 0 for a merged image of the donor (HA, green) and acceptor (FLAG, red) signal. The ROI (white box) was then photobleached, and graphical report of fluorescence intensity of donor (I) and acceptor (II) fluorescence from t = 0 to t = 145s is shown. (B) % FRET efficiency was calculated for the whole photobleached region for WT and mutant constructs. Figures are representative of one experiment with n = 9-10 for each experiment. The Kruskal-Wallis test was used for statistical analysis along with the two-tailed Mann-Whitney post-hoc test (* = $p < 0.05$).

Dimerization of WT D1D2 PTPRG decrease phosphatase activity

PTPRG D1D2 WT ($PTPRG^{WT}$) and PTPRG D1D2 DDKK ($PTPRG^{DDKK}$) protein purified from *E. coli* was used in pNPP kinetic assays in solution at low (10nM) and high (1uM) enzyme concentration. Under the assumption that dimerization inhibits the PTP activity, different kinetic parameters at the higher concentration of 1uM would confirm different abilities between the WT and DDKK mutant to dimerize. As expected, at the lower concentration of 10nM, $PTPRG^{WT}$ and $PTPRG^{DDKK}$ exhibited similar catalytic efficiencies with $kcat/K_M$ of 0.0106 $s^{-1}uM^{-1}$ and 0.0133 $s^{-1}uM^{-1}$, respectively (Figure 5A). However, once present in solution at a high concentration of 1uM $PTPRG^{WT}$ started showing an alternate curve pattern that could not be accurately fit to the Michaelis-Menten curve, while $PTPRG^{DDKK}$ fit a classic Michaelis-Menten curve with a K_M of 513.1uM and a $kcat/K_M$ of 0.0291 $s^{-1}uM^{-1}$ (Figure 5B). We hypothesized that this may be because in the initial stages of the reaction when the concentration of substrate is low, $PTPRG^{WT}$ is dimeric in solution such that the pNPP competes with monomeric $PTPRG^{WT}$ to bind/react with other monomeric $PTPRG^{WT}$; when the concentration of substrate increases, it is able to compete with $PTPRG^{WT}$ and push the reaction to a V_{max} that is similar to that of $PTPRG^{DDKK}$, which supposedly remains monomeric in solution (Barr et al., 2009). To confirm that high concentrations of $PTPRG^{WT}$ exhibited lower enzymatic activity and substrate specificity when substrate concentration is low, the pNPP kinetic assay was performed using 0-70uM of substrate. Figure 5C shows that $PTPRG^{WT}$ exhibited a lower catalytic efficiency (~⅓ less) compared to $PTPRG^{DDKK}$.

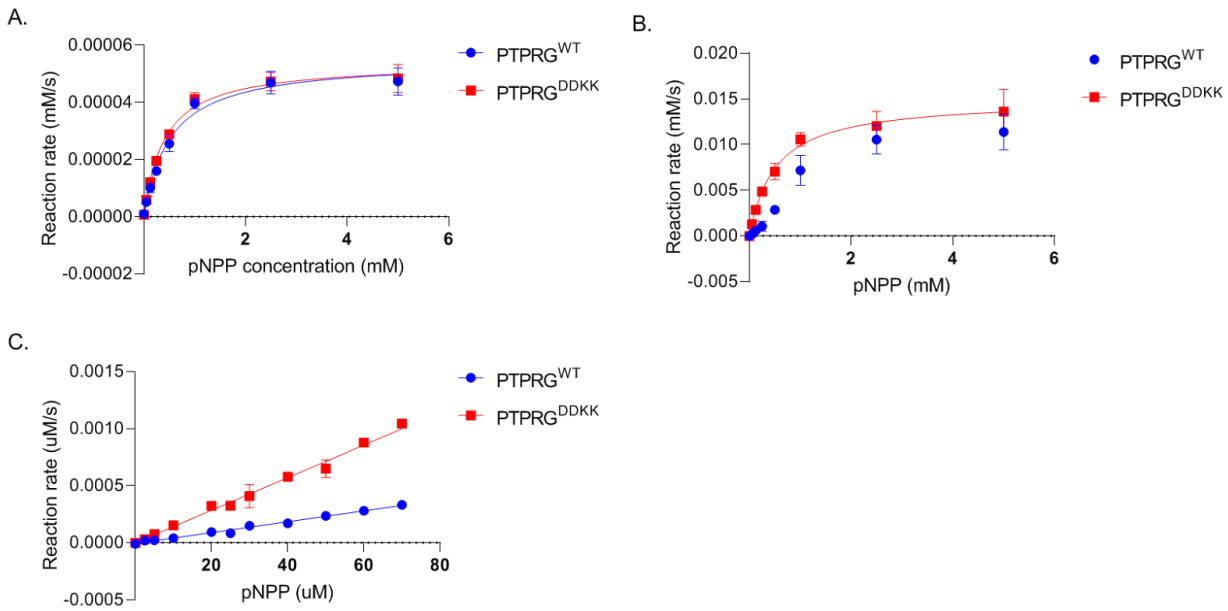

Figure 5: PTPRG^{DDKK} exhibits increased phosphatase activity compared to PTPRG^{WT} at high concentrations in solution. (A-B) Michaelis-Menten curve representing WT vs. DDKK PTPRG D1D2 enzyme activity of a (A) low concentration, 10nM, or (B) high concentration, 1uM, of protein using pNPP as a substrate at a range of 0-5mM. Data points are shown as mean ± standard deviation representative of three experiments. (C) Michaelis-Menten curve representing PTPRG^{WT} vs PTPRG^{DDKK} enzyme activity at a high concentration (1uM) using pNPP as a substrate at a range of 0-70uM. Data points are shown as mean ± standard deviation representative of three experiments.

DDKK mutation decreases D1D2 dimerization in vitro.

To confirm that PTPRG^{WT} was dimerizing more than PTPRG^{DDKK} in solution, a co-immunoprecipitation was performed using N-terminally FLAG or HA-tagged PTPRG D1D2 protein purified from *E. coli*, with the pull-down performed by the FLAG-PTPRG^{WT} protein. As shown in Figure 6, there was a greater HA-PTPRG^{WT} signal compared to the HA-PTPRG^{DDKK} signal, indicating that FLAG-PTPRG^{WT} pulled down HA-PTPRG^{WT} with greater efficiency than it did HA-PTPRG^{DDKK}.

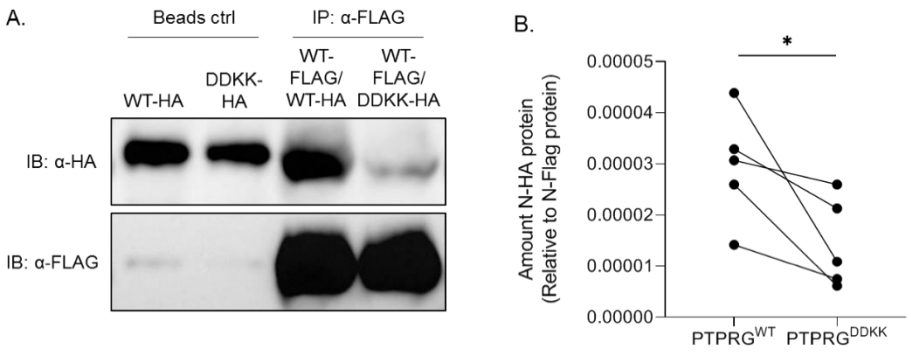

Figure 6: Co-immunoprecipitation of Flag- PTPRG^{WT} and HA- PTPRG$^{WT\ or\ DDKK}$. (A) A Co-IP assay was performed by incubating anti-FLAG conjugated beads with N-terminally FLAG-tagged PTPRG^{WT} followed by incubation with N-terminal HA-tagged PTPRG$^{WT\ or\ DDKK}$ to assess the pull-down of HA- PTPRG$^{WT\ or\ DDKK}$. HA- PTPRG$^{WT\ or\ DDKK}$ incubated with anti-FLAG conjugated beads alone were used as controls, and were used for normalization of signal in anti-HA blots. Blot is representative of 5 repeats. (B) Quantification of anti-HA signal relative to control and anti-FLAG signal from western blots. Data is shown as mean ± standard deviation representative of 5 experiments, and was analyzed using the two-tailed Mann-Whitney test (* = $p < 0.05$).

DISCUSSION

FRET microscopy, obtained and analyzed using various methods including pFRET, SEcFRET, and AP FRET, confirmed dimerization of WT PTPRG and the localization of dimeric protein at actin fibers in primary mDFs (Figures 2-4B). The dimerization-inactivating mutant DDKK showed comparatively diffuse FRET signaling patterns, weaker actin fibers, and decreased % FRET efficiency in both pFRET and AP FRET calculations (Figures 2, 3B, and 4B). These results suggest that the DDKK mutation successfully impaired overall protein dimerization in primary cells. The lack of defined actin structure seen in DDKK mutant samples (Figure 2) also suggests that PTPRG may play a role in actin fiber organization or stabilization. There are two possibilities: that the monomeric DDKK PTPRG can constitutively perform its phosphatase activity because it isn't suppressed through dimerization and this constitutive dephosphorylation activity leads to the destabilization of the actin structure, or that the PTPRG dimers somehow play a role in maintaining actin fiber stability in fibroblasts. Both these possibilities could be mediated through the interactions of monomeric or dimeric PTPRG with other proteins that act on actin.

In the first case, the ECD and transmembrane regions of PTPRG may still dimerize weakly even if the ICD of the protein is unable to dimerize (as in the case of the DDKK mutant); this has been observed in Protein tyrosine phosphatase type sigma (PTPRS), which, like PTPRG, has an ECD and a transmembrane region (Lee et al., 2007). If this is true of PTPRG, it is possible that this dimeric form of the DDKK protein would still provide a FRET signal (albeit at a lower efficiency because the proteins lack the added stability of ICD dimerization) while the protein still retains its phosphatase activity. This hypothetically uninhibited phosphatase activity could act on other proteins that typically nucleate, bundle, or polymerize actin fibers and deactivate them; this could create a downstream effect that leads to the destabilized actin fibers,

as seen in the DDKK phalloidin image in Figure 2. Gonzalez-Quedevo et al. found that Protein tyrosine phosphatase type sigma (PTPRS) interacts with Missing-in-Metastasis (MIM), a protein that regulates the actin cytoskeleton through F-actin bundling; this interaction was found to instigate cytoskeletal remodeling, which subsequently directs cellular migration and adhesion (2005). Another paper discovered that PTPRA interacts with α_v/β_3-integrin during early cell spreading, which facilitates the assembly of focal complexes and the strengthening of integrin-cytoskeleton bonds to allow for cellular migration and ECM remodeling by the cell (Gotz et al., 2003). Because cellular migration and ECM remodeling are distinct characteristics of fibrosis, if PTPRG regulates the actin cytoskeleton it could be a target to suppress fibrosis (Darby and Hewitson, 2007).

The data from the ΔECD mutant supports the idea that perhaps dimeric PTPRG plays a role in actin fiber stabilization, and also suggests that the ECD may play a role in regulating the localization of dimeric PTPRG in the cell. Figure 2 showed that cells transfected with ΔECD mutant exhibited FRET signal, but it didn't localize around actin fibers like WT and the CS mutant did; additionally, the actin fibers lacked a defined structure, which was similar to what we saw with the DDKK mutant. When the % FRET efficiency was quantified using pFRET analysis, the ΔECD mutant didn't show a significant increase in % FRET efficiency compared to WT protein (Figure 3B). In AP FRET, whole photobleached regions also didn't show significantly higher % FRET efficiency compared to WT protein. This is interesting because although removing the ECD doesn't significantly affect the relative amount of PTPRG dimerization, it causes decreased localization of the dimers on the actin cytoskeleton. Pairing this with the fact that we saw weaker actin fibers in these mutants (Figure 2), we could further explore the idea that the localization of PTPRG dimers affects the organization and structure of

the actin cytoskeleton. For instance, PTPRS also experiences ICD dimerization, and will only bind to ligands in their dimeric form (Lee et al., 2007). If this is true of PTPRG, then it is possible that some ligands will only bind dimeric PTPRG, which could lead to its localization on actin fibers.

Finally, the CS mutant had slightly lower levels of % FRET efficiency (Figure 3B) or similar levels of % FRET efficiency as WT PTPRG (Figure 4B). This indicated that when the enzyme is catalytically inactive, the dimerization of the protein potentially isn't drastically increased or decreased compared to catalytically active protein. The CS mutant also exhibited similar localization of dimeric protein on actin fibers as the WT protein (Figure 2). This could further support the idea that the localization of PTPRG dimers affects the actin cytoskeleton, rather than catalytic PTPRG activity. One issue with the results for CS is that % FRET efficiency calculated using pFRET was lower than that of WT, while in AP FRET there was no significant difference between the two; this discrepancy could be solved by performing other microscopy methods that are used to study protein-protein interactions, such as biofluorescence complementation assays (BiFC; will be explained in a later paragraph). This will help clarify whether the CS mutant consistently dimerizes at a lower rate than the WT protein or not. The FRET experiment could also be repeated in another PTPRG KO mDF cell line, which would provide additional information as to how PTPRG dimerization may differ across cells isolated from different PTPRG KO mice.

Moving forward, FRET microscopy can also be paired with time-course actin destabilization assays to explore if PTPRG dimers plays a role in actin fiber organization and/or stabilization. This can be performed by treating cells with cytochalasin, which is a class of fungal metabolites that inhibit actin polymerization (Casella et al., 1981); localization of FRET signal

can be traced over time to see how dimeric PTPRG mutants re-localize (or don't) to the actin fibers as they re-establish their structure. BiFC assays in both fixed and live samples could also bolster our current knowledge of the localization of PTPRG dimers. BiFC is a microscopy method also commonly used to study protein-protein interactions in which two non-fluorescent fragments of a fluorescent protein (ex. GFP) are fused to interacting proteins (in this case monomeric PTPRG; when the interacting proteins come into proximity of each other, the fluorescent fragments are able to re-form the fluorescent protein, and there is a fluorescent signal (Kerppola, 2008). BiFC in fixed samples will allow us to verify the previous FRET signals we saw in this study, and BiFC in live samples will allow us to visualize the real-time localization of dimeric protein in the cell. In this case, we could combine the actin cytoskeleton destabilization assay and live imaging of BiFC signal, visualizing if and where dimeric PTPRG localizes when the actin cytoskeleton is re-polymerizing. In any of these microscopy experiments, we can also stain for proteins that are known to reside and act on actin (through initiating actin polymerization, depolymerization, nucleation, etc.) such as cofilin, cortactin, or formin (Pollard, 2016).

In this study, biochemical assays helped discern the level of protein activity when a dimerization-impairing mutation was incorporated into PTPRG and helped us better understand the dimerization patterns of the ICD, as well as the phosphatase activity of the monomeric protein. Both $PTPRG^{WT}$ and $PTPRG^{DDKK}$ exhibited similar activity levels when present in solution at low concentrations (Figure 5A). However, when present in high concentrations in solution, the $PTPRG^{WT}$ showed a curve pattern that strayed from the expected Michaelis-Menten curve that it was expected to, while the mutant $PTPRG^{DDKK}$ fit the typical Michaelis-Menten model (Figure 5B). We hypothesized that this was because at high concentrations of protein,

$PTPRG^{WT}$ was dimerizing in solution while $PTPRG^{DDKK}$ was not. This meant that at low concentrations of pNPP, the substrate would have to compete with the $PTPRG^{WT}$ - $PTPRG^{WT}$ dimers in order to bind to the catalytic site; however, at saturating substrate concentrations, the substrate would be abundant enough to successfully compete with the dimers. We saw that this was the case as the final reaction rate for $PTPRG^{WT}$ and $PTPRG^{DDKK}$ were similar to each other (Figure 5B). To delve into our hypothesis about substrate competition with dimeric protein at low substrate concentrations, we performed the same assays with $PTPRG^{WT}$ and $PTPRG^{DDKK}$ protein and saw that $PTPRG^{DDKK}$ was indeed more catalytically active than $PTPRG^{WT}$ (Figure 5C). We verified that $PTPRG^{WT}$ was dimerizing and that the DDKK mutation was inhibiting protein dimerization in vitro through co-IPs with $PTPRG^{WT}$ and $PTPRG^{DDKK}$ in solution (Figure 6). Thus, we saw that the DDKK mutation interfered with the protein's ability to dimerize and that when in its dimeric form, the WT ICD of PTPRG shows less phosphatase activity.

What is still unknown about the role of PTPRG dimerization in fibroblasts is how pro-fibrotic stimulation may cause differential PTPRG activity and dimerization, and how this activity affects the phenotype of fibroblasts. A clear future direction is to perform assays in which PTPRG KO fibroblasts are transfected with WT or mutant PTPRG plasmids, then are stimulated with pro-fibrotic cytokines or growth factors such as TGF-β1 or IL-6. From there, the contractility, migration, or differentiation of fibroblasts/myofibroblasts can be studied using functional assays, such as scratch assays or collagen gel contraction assays.

BIBLIOGRAPHY

Alonso, A., Sasin, J., Bottini, N., Friedberg, I., Friedberg, I., Osterman, A., Godzik, A., Hunter, T., Dixon, J., & Mustelin, T. (2004). Protein Tyrosine Phosphatases in the Human Genome. *Cell*, *117*(6), 699–711. https://doi.org/10.1016/j.cell.2004.05.018

Andersen, J. N., Mortensen, O. H., PetersG. H., Drake, P. G., Iversen, L. F., Olsen, O. H., Jansen, P. G., Andersen, H. S., Tonks, N. K., & Møller, N. P. H. (2001). Structural and Evolutionary Relationships among Protein Tyrosine Phosphatase Domains. *Molecular and Cellular Biology*, *21*(21), 7117–7136. https://doi.org/10.1128/mcb.21.21.7117-7136.2001

Barr, A. J., Ugochukwu, E., Lee, W. H., King, O. N. F., Filippakopoulos, P., Alfano, I., Savitsky, P., Burgess-Brown, N. A., Müller, S., & Knapp, S. (2009). Large-Scale Structural Analysis of the Classical Human Protein Tyrosine Phosphatome. *Cell*, *136*(2), 352–363. https://doi.org/10.1016/j.cell.2008.11.038

Bastiaens, P. I., & Jovin, T. M. (1996). Microspectroscopic imaging tracks the intracellular processing of a signal transduction protein: fluorescent-labeled protein kinase C beta I. *Proceedings of the National Academy of Sciences*, *93*(16), 8407–8412. https://doi.org/10.1073/pnas.93.16.8407

Boni, C., Laudanna, C., & Sorio, C. (2022). A Comprehensive Review of Receptor-Type Tyrosine-Protein Phosphatase Gamma (PTPRG) Role in Health and Non-Neoplastic Disease. *Biomolecules*, *12*(1), 84. https://doi.org/10.3390/biom12010084

Casella, J. F., Flanagan, M. D., & Lin, S. (1981). Cytochalasin D inhibits actin polymerization and induces depolymerization of actin filaments formed during platelet shape change. *Nature*, *293*(5830), 302–305. https://doi.org/10.1038/293302a0

Chamberlain, C. E., Kraynov, V. S., & Hahn, K. M. (2000). Imaging spatiotemporal dynamics of Rac activation in vivo with FLAIR. *Methods in Enzymology*, 389–400. https://doi.org/10.1016/s0076-6879(00)25460-8

Chen, Y., Mauldin, J. P., Day, R. N., & Periasamy, A. (2007). Characterization of spectral FRET imaging microscopy for monitoring nuclear protein interactions. *Journal of Microscopy*, *228*(Pt 2), 139–152. https://doi.org/10.1111/j.1365-2818.2007.01838.x

Darby, I. A., & Hewitson, T. D. (2007). Fibroblast Differentiation in Wound Healing and Fibrosis. *International Review of Cytology*, *257*, 143–179. https://doi.org/10.1016/s0074-7696(07)57004-x

Day, R. N., Periasamy, A., & Schaufele, F. (2001). Fluorescence Resonance Energy Transfer Microscopy of Localized Protein Interactions in the Living Cell Nucleus. *Methods*, *25*(1), 4–18. https://doi.org/10.1006/meth.2001.1211

Del Pozo, M. A., Kiosses, W. B., Alderson, N. B., Meller, N., Hahn, K. M., & Schwartz, M. A. (2002). Integrins regulate GTP-Rac localized effector interactions through dissociation of Rho-GDI. *Nature Cell Biology*, *4*(3), 232–239. https://doi.org/10.1038/ncb759

Fujikawa, A., Sugawara, H., Tanga, N., Ishii, K., Kuboyama, K., Uchiyama, S., Suzuki, R., & Noda, M. (2019). A head-to-toe dimerization has physiological relevance for ligand-induced inactivation of protein tyrosine receptor type Z. *Journal of Biological Chemistry*, *294*(41), 14953–14965. https://doi.org/10.1074/jbc.ra119.007878

Gonzalez-Quevedo, R., Shoffer, M., Horng, L., & Oro, A. E. (2005). Receptor tyrosine phosphatase–dependent cytoskeletal remodeling by the hedgehog-responsive gene MIM/BEG4. *Journal of Cell Biology*, *168*(3), 453–463. https://doi.org/10.1083/jcb.200409078

Hansen, K. B., Staehr, C., Rohde, P. D., Homilius, C., Kim, S., Nyegaard, M., Matchkov, V. V., & Boedtkjer, E. (2020). PTPRG is an ischemia risk locus essential for HCO3−-dependent regulation of endothelial function and tissue perfusion. *ELife*, *9*. https://doi.org/10.7554/elife.57553

Hodgson, L., Shen, F., & Hahn, K. (2010). Biosensors for Characterizing the Dynamics of Rho Family GTPases in Living Cells. *Current Protocols in Cell Biology*, *46*(1). https://doi.org/10.1002/0471143030.cb1411s46

Iwamoto, N., Distler, J. H. W., & Distler, O. (2010). Tyrosine Kinase Inhibitors in the Treatment of Systemic Sclerosis: From Animal Models to Clinical Trials. *Current Rheumatology Reports*, *13*(1), 21–27. https://doi.org/10.1007/s11926-010-0142-x

Kendall, R. T., & Feghali-Bostwick, C. A. (2014). Fibroblasts in fibrosis: novel roles and mediators. *Frontiers in Pharmacology*, *5*(123). https://doi.org/10.3389/fphar.2014.00123

Kerppola, T. K. (2008). Bimolecular Fluorescence Complementation (BiFC) Analysis as a Probe of Protein Interactions in Living Cells. *Annual Review of Biophysics*, *37*(1), 465–487. https://doi.org/10.1146/annurev.biophys.37.032807.125842

Kraynov, V. S., Chamberlain, C., Bokoch, G. M., Schwartz, M. A., Slabaugh, S., & Hahn, K. M. (2000). Localized Rac activation dynamics visualized in living cells. *Science (New York, N.Y.)*, *290*(5490), 333–337. https://doi.org/10.1126/science.290.5490.333

Lee, S., Faux, C., Nixon, J., Alete, D., Chilton, J., Hawadle, M., & Stoker, A. W. (2007). Dimerization of Protein Tyrosine Phosphatase σ Governs both Ligand Binding and Isoform Specificity. *Molecular and Cellular Biology*, *27*(5), 1795–1808. https://doi.org/10.1128/MCB.00535-06

Maeda, N., Nishiwaki, T., Shintani, T., Hamanaka, H., & Noda, M. (1996). 6B4 Proteoglycan/Phosphacan, an Extracellular Variant of Receptor-like Protein-tyrosine Phosphatase ζ/RPTPβ, Binds Pleiotrophin/Heparin-binding Growth-associated Molecule (HB-GAM). *Journal of Biological Chemistry*, *271*(35), 21446–21452. https://doi.org/10.1074/jbc.271.35.21446

Meng, X., Nikolic-Paterson, D. J., & Lan, H. Y. (2016). TGF-β: the master regulator of fibrosis. *Nature Reviews Nephrology*, *12*(6), 325–338. https://doi.org/10.1038/nrneph.2016.48

Periasamy, A., Wallrabe, H., Chen, Y., & Barroso, M. (2008). Chapter 22: Quantitation of protein-protein interactions: confocal FRET microscopy. In *Biophysical Tools for Biologists, Volume Two: In Vivo Techniques*. CRC Press.

Pollard, T. D. (2016). Actin and Actin-Binding Proteins. *Cold Spring Harbor Perspectives in Biology*, *8*(8), a018226. https://doi.org/10.1101/cshperspect.a018226

Sacchetti, C., Bai, Y., Stanford, S. M., Di Benedetto, P., Cipriani, P., Santelli, E., Piera-Velazquez, S., Chernitskiy, V., Kiosses, W. B., Ceponis, A., Kaestner, K. H., Boin, F., Jimenez, S. A., Giacomelli, R., Zhang, Z.-Y., & Bottini, N. (2017). PTP4A1 promotes TGFβ signaling and fibrosis in systemic sclerosis. *Nature Communications*, *8*(1). https://doi.org/10.1038/s41467-017-01168-1

Shrestha, D., Jenei, A., Nagy, P., Vereb, G., & Szöllősi, J. (2015). Understanding FRET as a Research Tool for Cellular Studies. *International Journal of Molecular Sciences*, *16*(12), 6718–6756. https://doi.org/10.3390/ijms16046718

Sixt, M. (2012). Cell migration: Fibroblasts find a new way to get ahead: Figure 1. *The Journal of Cell Biology*, *197*(3), 347–349. https://doi.org/10.1083/jcb.201204039

Sun, Y., Rombola, C., Jyothikumar, V., & Periasamy, A. (2013). Förster resonance energy transfer microscopy and spectroscopy for localizing protein-protein interactions in living cells. *Cytometry Part A*, *83*(9), 780–793. https://doi.org/10.1002/cyto.a.22321

Tonks, N. K. (2006). Protein tyrosine phosphatases: from genes, to function, to disease. *Nature Reviews Molecular Cell Biology*, *7*(11), 833–846. https://doi.org/10.1038/nrm2039

Tzima, E. (2002). Activation of Rac1 by shear stress in endothelial cells mediates both cytoskeletal reorganization and effects on gene expression. *The EMBO Journal*, *21*(24), 6791–6800. https://doi.org/10.1093/emboj/cdf688

Tzima, E., Irani-Tehrani, M., Kiosses, W. B., Dejana, E., Schultz, D. A., Engelhardt, B., Cao, G., DeLisser, H., & Schwartz, M. A. (2005). A mechanosensory complex that mediates the endothelial cell response to fluid shear stress. *Nature*, *437*(7057), 426–431. https://doi.org/10.1038/nature03952

Vallée, A., & Lecarpentier, Y. (2019). TGF-β in fibrosis by acting as a conductor for contractile properties of myofibroblasts. *Cell & Bioscience*, *9*(1). https://doi.org/10.1186/s13578-019-0362-3

Wallrabe, H., Elangovan, M., Burchard, A., Periasamy, A., & Barroso, M. (2003). Confocal FRET Microscopy to Measure Clustering of Ligand-Receptor Complexes in Endocytic Membranes. *Biophysical Journal*, *85*(1), 559–571. https://doi.org/10.1016/s0006-3495(03)74500-7

Wichert G., Jiang, G., Kostic, A., De Vos, K., Sap, J., & Sheetz, M. P. (2003). RPTP-α acts as a transducer of mechanical force on αv/β3-integrin–cytoskeleton linkages. *Journal of Cell Biology*, *161*(1), 143–153. https://doi.org/10.1083/jcb.200211061

Wouters, F. S., Bastiaens, P., Wirtz, K., & Jovin, T. (1998). FRET microscopy demonstrates molecular association of non-specific lipid transfer protein (nsL-TP) with fatty acid oxidation enzymes in peroxisomes. *The EMBO Journal*, *17*(24), 7179–7189. https://doi.org/10.1093/emboj/17.24.7179

Wynn, T. (2008). Cellular and molecular mechanisms of fibrosis. *The Journal of Pathology*, *214*(2), 199–210. https://doi.org/10.1002/path.2277

Zal, T., & Gascoigne, N. R. J. (2004). Photobleaching-Corrected FRET Efficiency Imaging of Live Cells. *Biophysical Journal*, *86*(6), 3923–3939. https://doi.org/10.1529/biophysj.103.022087

Zehender, A., Huang, J., Györfi, A.-H., Matei, A.-E., Trinh-Minh, T., Xu, X., Li, Y.-N., Chen, C.-W., Lin, J., Dees, C., Beyer, C., Gelse, K., Zhang, Z.-Y., Bergmann, C., Ramming, A., Birchmeier, W., Distler, O., Schett, G., & Distler, J. H. W. (2018). The tyrosine phosphatase SHP2 controls TGFβ-induced STAT3 signaling to regulate fibroblast activation and fibrosis. *Nature Communications*, *9*(1). https://doi.org/10.1038/s41467-018-05768-3

Zhang, Y. E. (2008). Non-Smad pathways in TGF-β signaling. *Cell Research*, *19*(1), 128–139. https://doi.org/10.1038/cr.2008.328